JOURNAL OF MATERIALS SCIENCE 26 (1991) 6408–6418

Optical properties and chemical reactivity of hydrogenated amorphous boron thin films

C. GODET
Laboratoire de Physique des Interfaces et des Couches Minces (UPR A 0258-CNRS), Ecole Polytechnique, F-91128 Palaiseau Cedex, France

L. SCHMIRGELD*, L. ZUPPIROLI
Laboratoire des Solides Irradiés, Ecole Polytechnique, F-91128 Palaiseau Cedex, France

G. SARDIN
Departament de Fisica Aplicada i Electronica, Universitat de Barcelona, Avenida Diagonal 645, E-08028 Barcelona, Spain

S. GUJRATHI, K. OXORN
Laboratoire de Physique Nucléaire, Université de Montréal, case postale 6128, succursale A, Montréal, Québec Canada H3C 3J7

Hydrogenated boron thin films have been deposited at temperatures in the range 50–100 °C with the radiofrequency plasma decomposition of diborane B_2H_6 diluted in hydrogen. The chemical composition of the films has been determined by elastic recoil detection and by the Castaing microprobe techniques. We have found that the as-deposited films contain 10–20 at % H and that they react with the ambient atmosphere within a few days and reach a final composition close to $B_{0.64}H_{0.12}O_{0.12}C_{0.06}N_{0.06}$. The optical properties of the as-deposited films studied by spectroscopic phase-modulated ellipsometry in the range 1.7–5.0 eV are characteristic of the high optical gap semiconductors. The electron diffraction measurements performed on *in situ* annealed samples show that the films are amorphous up to 950 °C. Infrared spectroscopy investigations performed on the as-deposited films have revealed two hydrogen bonding sites: B–H terminal bonds and B–H–B bridge bonds, along with some B–O–B groups. Upon exposure to the atmosphere, the vanishing of B–H–B and B–O–B bridge bonds and the increase of B–H and B–O–H absorption bands after 1 day, are observed.

1. Introduction

Hydrogenated amorphous boron (a-B:H) thin films have been studied for their potential use as protective coatings in nuclear fusion reactors [1, 2], hard coatings [3] and semiconductor material for large-area photovoltaic conversion devices [4, 5]. The introduction of hydrogen atoms in the boron network has been achieved either by diborane B_2H_6 pyrolysis [5] and plasma-assisted chemical vapour deposition [2, 4, 6, 7], or by electron beam evaporation of boron in a residual hydrogen atmosphere [8]. Very large amounts of incorporated hydrogen atoms have been revealed by infrared absorption [1, 6, 8], ^{15}N nuclear reaction [1, 5] and hydrogen thermal effusion [6], up to 30% and 45%, respectively, at deposition temperatures of 270 and 30 °C [6].

Amorphous elemental boron, as well as the different allotropic modifications of crystalline boron, contains B_{12} icosahedra held together by strong intericosahedral covalent bonds [9]. The structural investigation of boron–hydrogen alloys may give a better insight into the changes due to the hydrogen atoms in the complex arrangement of B_{12} units and their chemical stability. In particular, it is wondered if hydrogen atoms could act as bond terminators and relieve the internal strains, as observed, for example, in hydrogenated amorphous silicon [10]. Experimentally, infrared transmission spectra reveal that hydrogen can occupy two kinds of sites in a-B:H alloys: a bridging hydrogen site (three-centre B–H–B bond) or a terminal site (B–H bond), as also occurs in the B_2H_6 molecule [11]. The bridge bonding site becomes predominant as the material changes from a polymeric boron-hydride to a highly cross-linked amorphous network [6] as a result of changing the deposition parameters [7]. However, an increase of the hydrogen incorporation as moisture into films deposited at temperatures lower than 300 °C has been observed upon exposure to air [2, 12].

This paper reports the study of a-B:H thin films deposited at temperatures in the range 50–100 °C by the glow-discharge decomposition of B_2H_6 diluted in

*On leave from Physics Department, CNEA, Avenida Libertador 8250, 1429 Buenos-Aires, Argentina, and CONICET. *Present address*: Service de Recherche de Métallurgie Physique, CEA, Saclay, 91191 Gif-sur-Yvette, France.

0022–2461/91 $03.00 + .12

hydrogen. The spectroscopic ellipsometry technique gives evidence of a high optical gap, together with a low absorption coefficient in the visible spectrum, related to the high hydrogen content revealed by infrared spectroscopy, elastic recoil detection analysis and thermal effusion measurements. A quantitative analysis of the infrared spectra is performed in order to evaluate the relative contributions of the B–H terminal bonds and the B–H–B bridge bonds. The important modifications resulting from the high reactivity of a-B:H films upon atmospheric exposure are discussed in relation to the boron and hydrogen atomic densities and to the quantitative analysis of the impurity incorporation. Some complementary measurements on a-B:C:H films, obtained from $B(CH_3)_3$ diluted in hydrogen, are used in order to check the influence of carbon incorporation and the validity of the optical model.

2. Experimental procedure

The hydrogenated amorphous boron films, 0.1–1.1 μm thick, were deposited using the ARCAM reactor [13] on silica (SiO_2) and single-crystal silicon (c-Si) substrates by the radiofrequency (r.f.) 13.56 MHz glow-discharge decomposition of diborane B_2H_6 (99.99%) diluted with hydrogen (99.9995%) at a 0.52% level. The total flow rate, pressure and r.f. power were set to 114 standard $cm^3\ min^{-1}$, 0.30 torr and 5 W (0.05 W cm^{-2}), respectively, in order to sustain the plasma. At the typical deposition temperatures, $T_s = 50$–100 °C, used in this study, the base pressure was lower than 5×10^{-7} torr. The hydrogenated boron carbide material was deposited at 250 °C from trimethylboron $B(CH_3)_3$ diluted at 1% in hydrogen. In both cases, no significant thermal decomposition of B_2H_6 at 100 °C or of $B(CH_3)_3$ at 250 °C were observed.

After the samples were cooled in a nitrogen atmosphere, the dielectric function spectra were measured in the 1.7–5.0 eV range with a spectroscopic phase-modulated ellipsometer (SPME) described previously [14]. The a-B:H thin films looked like a nearly transparent and slightly diffusing material when deposited on silica substrates, while the samples on c-Si substrates reflected different visible photon wavelengths depending on the film thickness. This multiple interference effect was also observed in the SPME spectra and taken into account to determine the film thickness, the true dielectric function, and to obtain the static refractive index and the mean optical gap (Section 3.1). The samples deposited on c-Si were immediately transferred into a Nicolet MX-5 Fourier transform infrared spectrometer and the transmission in the range 400–4000 cm^{-1} was measured after 10 min in the ambient atmosphere. Then the samples were stored either in the ambient atmosphere or under a primary vacuum; in both cases, the evolution of the infrared spectra due to air exposure described in Section 3.2 is qualitatively the same, with a slower kinetics in the latter case.

The chemical analysis of some amorphous boron thin films described in Section 3.3 was performed a few months after the deposition, either by the Castaing microprobe technique or by the elastic recoil detection (ERD) using ^{35}Cl as the probing ions. The number of hydrogen atoms was obtained from ERD, thermal effusion and infrared transmission. The thermal effusion measurements have been performed in a quartz tube with a static vacuum of 10^{-3} torr. The samples deposited on c-Si were heated up to 750 °C with a heating rate of 0.3 $K\ s^{-1}$ and the evolution of the hydrogen partial pressure was measured with a quadrupolar mass spectrometer Quadruvac Q200 Leybold–Heraeus [15]. The Castaing microprobe experiments were performed under a 10^{-6} torr vacuum. The electron bombardment induced X-ray emission lines for boron and oxygen atoms were measured for ten electron energies in the range 1.5–15 keV in order to obtain information on the composition [16], in particular the atom density ratio O/B. The elastic recoil detection experiment described by l'Ecuyer *et al.* [17] allows the determination of the chemical composition profiles for all the light elements, including hydrogen, by combining the elastic recoils ejected by a beam of ^{35}Cl ions and the time-of-flight (TOF) technique [18, 19]. The energy distribution of the recoiled particles, as well as the scattered ions results from the energy losses as the incident ions penetrate the target and as they emerge from the target after the elastic collision. The energy loss rate is a function of the ion energy and the composition of the target. The hydrogen atom content was obtained by comparing the signals given by a surface barrier detector with and without a mylar absorber. In order to find the concentration of the other elements, another measurement was performed by the ERD–TOF technique, giving first the mass spectrum of the target, then the individual energy spectra by using mass windows, the latter being finally deconvoluted to obtain the depth-profiles of the individual elements without any a priori assumptions about the composition of the unknown target [20]. The absolute atomic densities are obtained using, as references, the c-Si substrate atomic density (5×10^{22} at cm^{-3}) and the absolute film thickness deduced from the ellipsometry measurements.

3. Results and discussion

3.1. Spectroscopic ellipsometry

The spectroscopic phase-modulated ellipsometry (SPME) technique was used to characterize the boron thin films in the as-deposited state. The optical properties of two samples deposited on SiO_2 and single-crystal silicon, respectively, at 100 and 50 °C, are analysed.

Fig. 1 shows the real and imaginary parts of the pseudo-dielectric function of a film deposited at 100 °C on an SiO_2 substrate. The interference patterns result from the multiple internal reflections in the a-B:H film, which means that the inverse absorption coefficient in the visible–near ultraviolet spectrum is higher than the sample thickness. In the optical model, the rear-face frosted substrate is considered to be semi-infinite and the film–air interface to be abrupt. The film thickness, d, and the dielectric function, $\varepsilon(E) = \varepsilon_1$

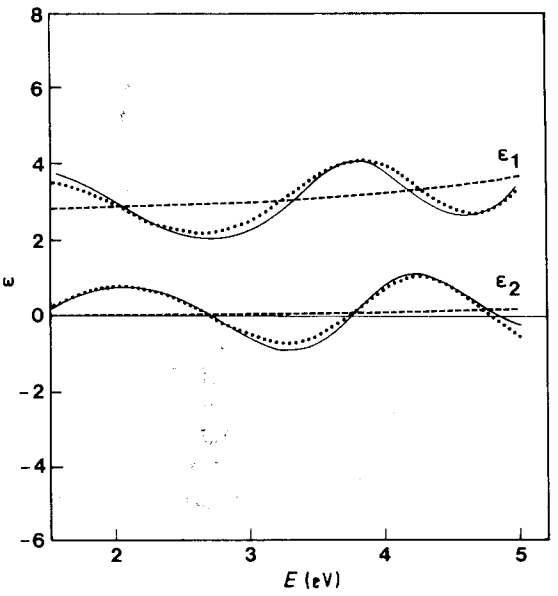

Figure 1 Real and imaginary parts of the dielectric function of a-B:H deposited on SiO_2 at $T_s = 100\,°C$ (——). The simulated curve (· · ·) is obtained by using a single damped harmonic oscillator function (– – –).

$-i\varepsilon_2$ of the material are obtained by assuming that the latter can be described by a single damped harmonic oscillator [21] in the experimentally available energy range, well below the optical gap. The theoretical expression of the real and imaginary parts of $\varepsilon(E)$ as a function of the photon energy, E, is given by

$$\varepsilon_1(E) = 1 + A(E_G^2 - E^2)/\Gamma^2E^2 + (E_G^2 - E^2)^2 \quad (1)$$

$$\varepsilon_2(E) = A\Gamma E/(E_G^2 - E^2)^2 + \Gamma^2E^2 \quad (2)$$

where A, E_G, Γ are, respectively, the oscillator strength, the resonance energy (or mean optical gap) and the damping factor. Then the static refractive index may be written as

$$n_0 = (1 + A/E_G^2)^{1/2} \quad (3)$$

The standard minimization procedure described previously [22] leads to a good agreement of the calculated spectra (Fig. 1, dotted line) with the experiment; the least-squares sum $\delta^2_{min} = 4 \times 10^{-2}$ is obtained for the following values of the four parameters: $A = 125\ eV^2$, $\Gamma = 0.81$ eV, $E_G = 8.4$ eV which characterize the theoretical dielectric function (dashed line) and $d = 158$ nm. No improvement could be obtained by introducing in the model a rough layer at the film–air interface. The deposition rate, $V_d = 0.014\ nm\,s^{-1} = 0.05\ \mu m\,h^{-1}$ and the static index $n_0 = 1.664$ follow immediately from the fitted parameters. According to this model, the energy $E_{04}(E_{03})$ corresponding to the absorption coefficient $\alpha = 10^4\ cm^{-1}$ ($10^3\ cm^{-1}$) is found to be 3.45 eV (1.2–1.5 eV).

As the a-B:H film index is not very different from that of the SiO_2 substrate, a low-amplitude interference pattern is observed in Fig. 1. In the case of c-Si substrates, the amplitude is much higher, as revealed by the pseudo-dielectric function displayed in Fig. 2. The fringes are more closely spaced due to the higher deposition time and film thickness. Using the same

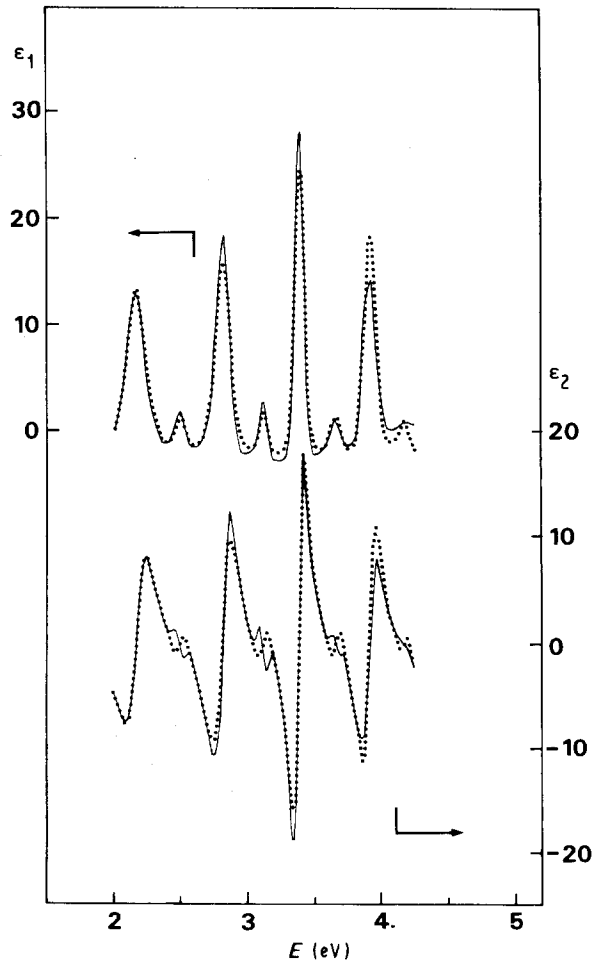

Figure 2 Experimental (——) and simulated (· · ·) dielectric functions of a-B:H deposited on c-Si at $T_s = 50\,°C$.

model as in the previous case and the dielectric function of c-Si measured by Aspnes and Studna [23], a rather rough agreement ($\delta^2_{min} = 3.3$) is obtained with the best-fitting parameters: $A = 110\ eV^2$, $\Gamma = 0.33$ eV, $E_G = 8.1$ eV and $d = 617$ nm, provided the spectral range be restricted to energies lower than 4.25 eV. The deposition rate $V_d = 0.014\ nm\,s^{-1}$ and the static index, $n_0 = 1.634$, compare very well to the previous results although the deposition temperature is lower in the latter case. The minor discrepancy when ε_2 crosses the baseline remains unexplained. The optical gap resulting from this model, $E_{04} = 4.15$ eV, is higher than the value obtained with the film deposited at 100 °C, $E_{04} = 3.45$ eV. After a few months in the ambient atmosphere, this same sample shows slightly modified optical properties (calculated with the same optical model) in the visible–near ultraviolet range: the mean optical gap and the static index are increased to $E_G = 8.9$ eV and $n_0 = 1.72$, respectively. Below the optical gap, the photothermal deflection spectroscopy measurements on a sample exposed to the atmosphere show that the absorption coefficient $\alpha(E)$ profile in the 1.0–2.5 eV range may be described by an exponential Urbach edge characterized by the inverse slope $E^\circ = 550$ meV.

The influence of carbon incorporation on the optical properties may be inferred from the boron–carbon alloy; the standard analysis performed in the

1.7–4.0 eV range for a-B:C:H deposited on SiO_2 leads to the following parameters: $A = 120\,eV^2$, $\Gamma = 1.40\,eV$, $E_G = 7.12\,eV$. The calculated SPME thickness, $d = 415\,nm$, compares well to the stylus profiling result of 429 nm; the corresponding deposition rate is $V_d = 0.01\,nm\,s^{-1}$. The higher value of $n_0 = 1.83$ and lower $E_G = 7.12\,eV$, as compared to a-B:H films, may be attributed to the higher C/B ratio in the alloy of composition $B_{0.34}C_{0.31}O_{0.01}H_{0.34}$ (see Section 3.3.1).

The results for the optical properties of our hydrogenated amorphous boron films can be summarized by the optical gaps E_{04} in the range 3.4–4.2 eV, E_{03} below 1.5 eV and the static refractive index $n_0 = 1.63$–1.67. The optical gap increases as the deposition temperature decreases, which may be attributed to an increase in the hydrogen content (Section 3.3.3). These data can be compared to previous studies of a-B:H films with different hydrogen contents: a higher absorption characterized by $n_0 = 3$, and $E_{03} = 0.8$ eV has been reported for amorphous boron with a low hydrogen impurity content [24]; in contrast, the value $E_{03} = 2.3$ eV has been found for boron films with 42 at % hydrogen obtained by the glow-discharge decomposition of diborane [25]. The first conclusion is that these results are consistent with the positive correlation previously found between the optical gap E_G and the hydrogen content in chemical vapour deposited (CVD) boron–hydrogen alloys [5]. However, the high hydrogen content (around 30%) and the comparatively low optical gap ($E_{03} = 1.3$ eV and $E_{04} = 1.9$ eV) found in some anodic glow-discharge films deposited at 270 °C [6] seem to belie this general trend. Second, the increase of the refractive index upon both atmospheric exposure and carbon alloying are consistent with the incorporation of chemical elements (C, N, O) heavier than boron.

3.2. Infrared absorption

3.2.1. Experimental results and peak assignment

The typical infrared absorption spectra of a-B:H films measured within 0.1 h after deposition are shown in Fig. 3a and b. In addition, Fig. 3c–e and Fig. 4a–d display the evolution of the infrared absorption when the films are exposed to the ambient atmosphere.

The main reproducible features of the as-deposited films (a) are strong absorption band at 2560 cm^{-1} along with two very broad bands centred around 2050 and 1380 cm^{-1}, followed at lower wavenumbers by at least four very weak bands at 1075, 905, 740 and 565 cm^{-1}. In the as-deposited films (a) and (b), no absorption feature can be detected above the 2560 cm^{-1} band and the feature at 2350 cm^{-1} is an artefact due to the CO_2 background. By comparison with the diborane absorption [11] and previous studies of a-B:H alloys thin films [6, 8], the sharp 2560 and broad 2050 cm^{-1} bands are readily attributed to the terminal B–H bond stretching and the B–H–B bridge bond absorption, respectively. However the spectra of the as-deposited material show no clear evidence of the 1108 cm^{-1} band previously attributed to the B–H bending mode [5]. The broad band observed at 1380 cm^{-1} in the as-deposited films can be assigned to the B–O stretching vibration in the B–O–B group as observed in dry boron oxide B_2O_3 films [26]; this assumption implies the incorporation of oxygen atoms during film

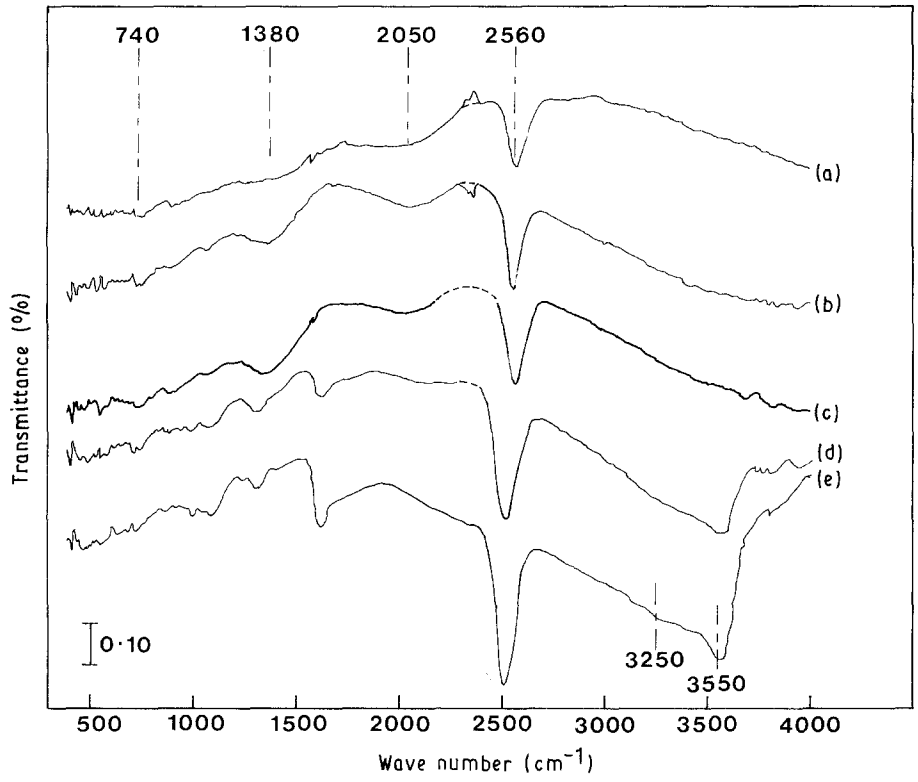

Figure 3 Infrared transmission spectra of as-deposited (0.1 h in the ambient atmosphere) a-B:H films ($T_s = 100$ °C) on c-Si with different thickness: (a) 0.68 μm, (b) 0.97 μm. (c–e) Spectra taken on the same film (1.10 μm) after 6, 72 and 120 h exposure, respectively, to the ambient atmosphere.

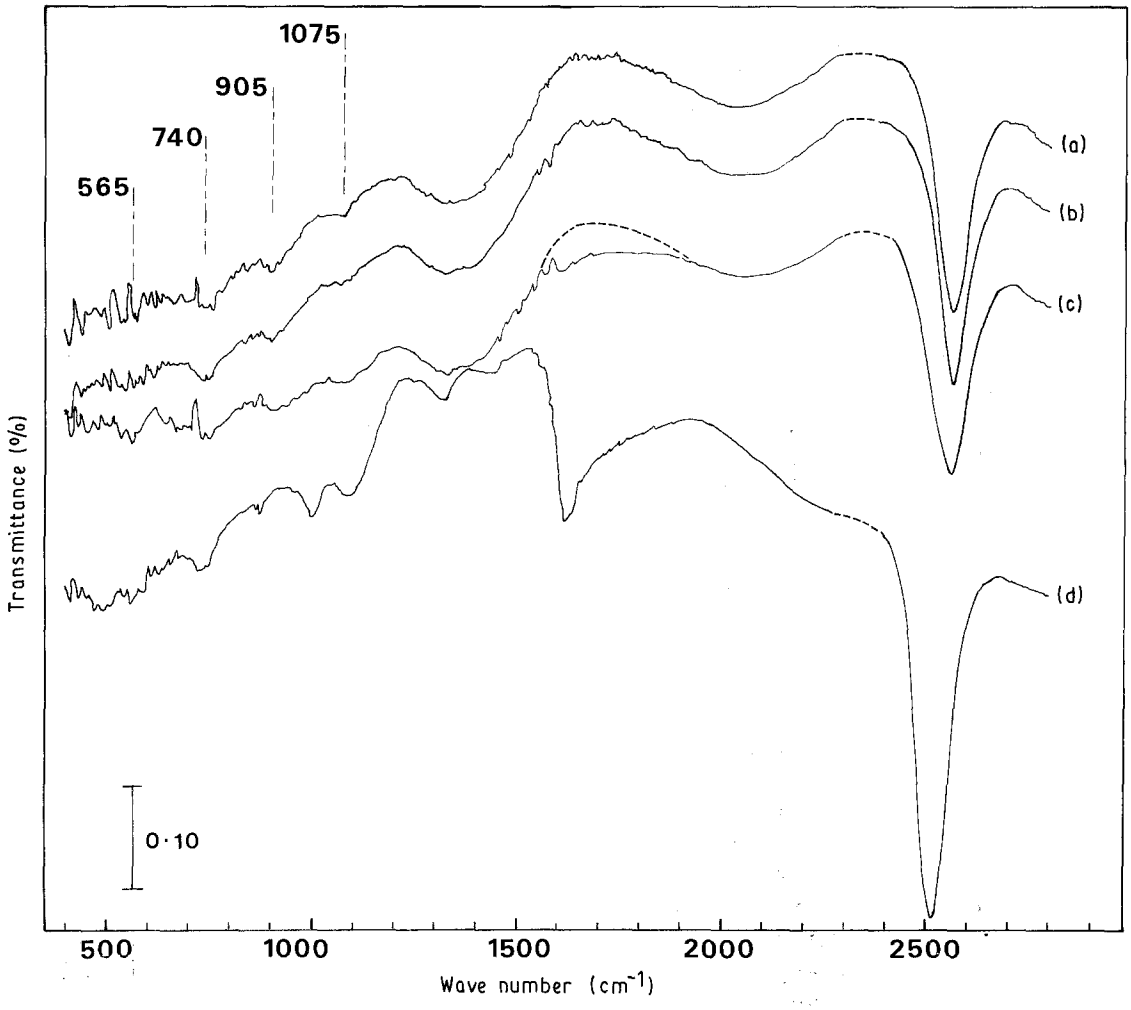

Figure 4 Infrared transmission spectra of a 0.97 μm thick a-B:H film (T_s = 100 °C) exposed to the ambient atmosphere for (a) 0.5 h, (b) 1 h, (c) 24 h and (d) 680 h.

growth, estimated to a few per cent at least. Finally, the series of four absorption bands below 1100 cm^{-1} (Fig. 4) roughly corresponds to previous observations by Tsai on glow-discharge anodic a-B:H samples prepared at T_s = 25 °C [6]. These peaks are attributed to the boron lattice vibrations, and will be discussed below (Section 3.2.2).

Strong modifications are observed after a few days at the ambient atmosphere, in particular we emphasize the following points.

(i) Fig. 3 shows an increase of an asymmetric band with at least two components located at 3250–3550 cm^{-1}; this band is attributed to the bonding of OH groups to boron atoms [26, 27] as a result of the atmosphere exposure. A preliminary explanation of a two-component O–H absorption feature could be the occurrence of B–O–H groups located both in the bulk and on the surface of the film [27]. A broadening of the bulk feature may be expected as a consequence of the distribution of bond strengths due to the disorder and the sterical effects in the amorphous network. Then, the relative importance of the "surface" and "bulk" absorption bands would indicate that the a-B:H films investigated in the present report do present an important void network. An alternative explanation can be inferred from the previous study of the infrared absorption of the vitreous boric oxide as a function of the water content [26]: a 3226 cm^{-1} band was attributed to the surface formation of boric acid upon water adsorption, while a 3580 cm^{-1} band was found in the spectrum of dry boron oxide glass. The latter explanation is preferred because after a few months of atmospheric exposure similar intensities and linewidths are observed for both components.

(ii) Similarly, the B–O stretching mode in the B–O–H groups can be assigned tentatively to the broad 1750 cm^{-1} and thin 1620 cm^{-1} components of another asymmetric band shown in Fig. 3e. Fig. 4c and d show the initial increase of the absorption near 1620 cm^{-1}. Therefore, the reaction with the ambient atmosphere is significant at the scale of 1 day.

(iii) In the low wave number range, among the four weak bands below 1100 cm^{-1} observed in the as-deposited material, only the 740 and 565 cm^{-1} bands remain clearly observable after a 1 month exposure to the ambient atmosphere (Fig. 4d). The growth of four absorption bands located at 1430, 1315, 1090 and 1000 cm^{-1} is also evident (Fig. 4d). The latter two frequencies compare quite well with the calculated ones (1087 and 1002 cm^{-1}) for the B–O–B molecule [28]. However, the feature observed at 1090 cm^{-1} corresponds to the expected bending vibration of the OH group found at 1080 cm^{-1} in boron oxide glass [26].

(iv) In addition, the 2560 cm^{-1} band due to B–H bonds increases in an important way and shifts to

lower wave numbers (down to 2510 cm^{-1}). As the boron–hydrogen alloys undergo the hydroxylation reaction, the chemical environment of the terminal B–H bonds is modified; the increase in the effective mass with the incorporation of oxygen atoms may qualitatively explain the shift of the 2560 cm^{-1} band to lower frequencies.

(v) Finally, the intensity of the band attributed to B–O–B groups at 1380 cm^{-1} does not increase and even vanishes as the film is exposed to the atmosphere. The same behaviour is found for the 2050 cm^{-1} broad band due to the B–H–B bridges bonds.

In summary, from the increase of the 3250 and 3550 cm^{-1} components of the high wave number band, we have deduced the bonding of O–H groups to boron atoms as a result of exposure to the atmosphere. The enhancement of the B–H absorption (2560 cm^{-1}) and the decrease of the B–H–B and B–O–B bridges are considered to be indications of a global decrease of the cross-linking in the network. Then, from the modifications of the a-B:H absorption spectrum upon exposure to the ambient atmosphere, we attribute the important creation of B–O–H and B–H groups to an hydrolysis process. In contrast, no incorporation of $C–H_n$ bonds, which are expected to appear in the 2850–2950 cm^{-1} range, has been detected, but the formation of B–C bonds cannot be excluded.

3.2.2. Lattice vibrations

Let us turn now to a structural analysis of the lattice vibrations observed in the as-deposited films. As the icosahedral B_{12} units have been evinced in all the various modifications of crystalline elemental boron and in some evaporated amorphous films [9, 29], we are led to assume that the B_{12} icosahedron remains the basic unit in our amorphous hydrogenated films. This point is also addressed in Section 3.3.4. In this icosahedral frame, the structure of hydrogenated a-B:H alloys may be tentatively compared to that of the $B_{12}H_{12}^{2-}$ anion; the molecular vibrations of $B_{12}H_{12}^{2-}$ have been studied theoretically by Weber and Thorpe [30] on the basis of infrared and Raman scattering experiments. In this way, complementary results were obtained on the forces acting within the icosahedron (intra-bonding) and on the forces between boron and hydrogen atoms, related to the inter-icosahedral coupling. Among the best models used by Weber and Thorpe to describe the coupling between first- and second-neighbour atoms, model V in [30] gives phonon frequencies at 565, 739–744, 964, 1045 and 2520 cm^{-1} quite similar to our experimental data (Fig. 4). The main characteristic of this model is a considerable asymmetry between the non-central forces acting in the icosahedral surface and perpendicular to it, because the latter is stronger and highly directional.

3.2.3. Quantitative analysis of the bonded hydrogen

Two estimations of the bonded hydrogen content were performed using the infrared spectroscopy data. First, a rough quantitative estimation of the hydrogen atom content may be realized by using a correlation established by Blum between the terminal hydrogen atoms 2560 cm^{-1} infrared absorption and the total hydrogen content obtained by secondary ion mass spectroscopy (SIMS) measurements on evaporated boron films [8]. In the limit of concentrations lower than a few per cent, a Beer–Lambert analysis of the infrared transmittance, T_{IR}, leads to the expression

$$[H_{SIMS}] = (0.578/d(\mu m))\ln(1/T_{IR}) + 0.006 \quad (4)$$

Assuming that this law holds for higher hydrogen contents, the transmittance at 2560 cm^{-1} in the spectrum in Fig. 4b before atmospheric exposure leads to 12.4 at % H which corresponds to a maximum value of 1.6×10^{22} H atoms cm^{-3} if the boron atomic density of the evaporated films in [8] is comparable to that of the crystal (13×10^{22} B atoms cm^{-3}). The same analysis yields a hydrogen content of 4.0×10^{22} H atoms cm^{-3} after 680 h in the ambient atmosphere.

Second, a more detailed analysis can be performed by the integration of the 2560 and 2050 cm^{-1} bands, following the method described in [31]. The integrated absorption I defined as: $I = \int \alpha(\omega)\,d\omega$, for the bridge bonds ($I = 2.68 \times 10^5$ cm^{-2}) and the terminal bonds ($I = 1.98 \times 10^5$ cm^{-2}) absorption bands of the as-deposited film (Fig. 4b) are nearly equal and their sum compares well to the terminal bonds absorption ($I = 4.80 \times 10^5$ cm^{-2}) in the atmosphere exposed sample (Fig. 4d). In principle, the density of B–H bonds can be deduced from the integrated absorption, I, material static index, n_0, light velocity c, reduced mass $m(B - H) = 0.92$ and the effective charge, e_s^* (respectively e_g^*) of the B–H bond in a medium of dielectric constant ε_m (respectively 1 in the diluted gas) according to the equation [31]

$$N_{B-H} = \frac{cn_0 m(B - H)}{2\pi^2 e_s^{*2}} I \quad (5)$$

However, in the solid phase, the local field differs from the applied external electromagnetic field so that the relation between the dielectric constant of the medium and the oscillator strength is not straightforward. As discussed previously in the case of hydrogenated amorphous silicon [32], this local field enhancement depends on the shape of the cavity in which each dipole is placed. The two extreme cases, namely, a spherical cavity and a "flat pill-box" cavity, can be considered theoretically. Then, the local field factor, e_s^*/e_g^*, ranges from $3\varepsilon_m/(1 + 2\varepsilon_m)$ to ε_m, respectively. Using the same value as in [33] ($e_g^* = 0.2$) and the static index deduced from the SPME measurements ($\varepsilon_m = n_0^2 = 2.77$) leads to a proportionality constant N_{B-H}/I ranging from 4.9×10^{16}–2.3×10^{17} cm^{-1}, that is within a range of a factor of 5. The lower value obtained in the "flat pill-box" approximation may be arbitrarily chosen because it yields hydrogen contents closer to those deduced from ERD or effusion experiments (Section 3.3.3). The basic reason why this particular oscillator strength should be chosen remains unclear. In addition, assuming that the bridge bond and terminal bond oscillator strengths are the

same, the respective amounts of BHB and BH arrangements are found to be 1.3×10^{22} H atoms cm^{-3} and 1.0×10^{22} H atoms cm^{-3} in the as-deposited films. Using the boron atomic density measured by ERD (Section 3.3), these values yield a global ratio H/B = 0.38 slightly higher than the same ratio obtained from the Beer–Lambert analysis (H/B = 0.27). In the atmospherically exposed material, the terminal hydrogen atomic density amounts to 2.4×10^{22} H atoms cm^{-3} and the bridge-bond component is comparatively small, so that the ratio H/B = 0.40 is deduced. As a partial conclusion, the above results, if qualitatively unambiguous, suffer some large quantitative uncertainties arising from the ill-defined effective charge and local field factor in the solid phase.

3.3. Chemical composition and structural analysis

3.3.1. Elastic recoil detection (ERD)

Fig. 5 shows the mass spectrum and composition profile of a thin film deposited on c-Si at 50 °C and exposed to the atmosphere for 12 months. First, the ^{10}B and ^{11}B isotopes are seen along with an important contribution of impurities such as ^{12}C, ^{14}N and ^{16}O. The ^{28}Si contribution due to the substrate and the

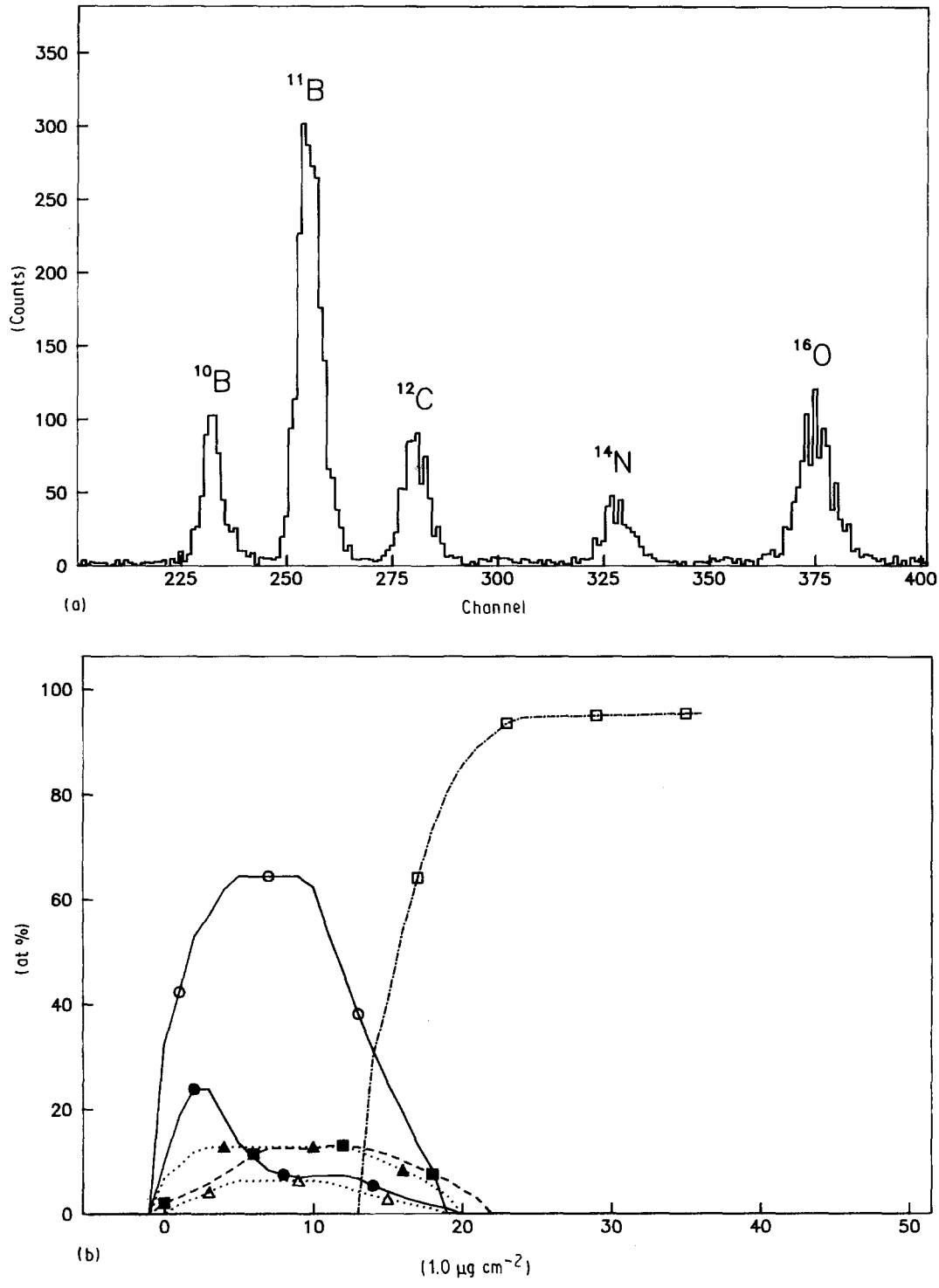

Figure 5 (a) ERD mass spectrum, (b) TOF–ERD profiles for an hydrogenated amorphous boron sample deposited at 50 °C on c-Si and exposed to atmosphere for 12 months. The thickness deduced from the SPME spectrum is 106 nm: (○) B, (●) C, (△) N, (▲) O, (□) Si, (■) H.

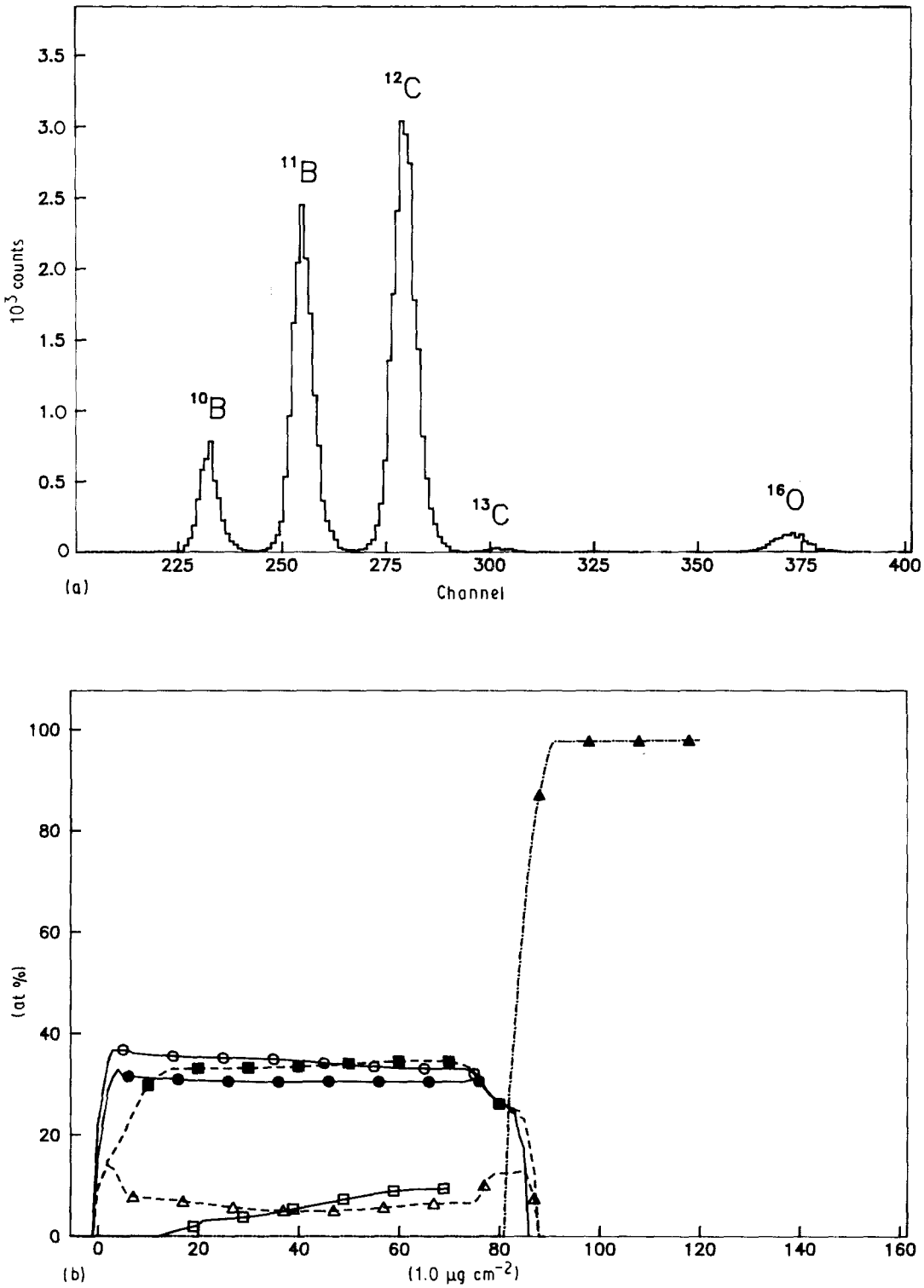

Figure 6 (a) ERD mass spectrum, (b) TOF–ERD profiles (at %) for an amorphous boron–carbon–hydrogen alloy deposited at 250 °C on c-Si and exposed to atmosphere for 1 month. The thickness deduced from the SPME spectrum is 415 nm: (○) B, (●) C, (△) O (× 5), (▲) Si, (□) Cr (× 20), (■) H.

^{35}Cl line corresponding to the ion beam are not shown. A small amount of atomic chromium around the channel 630 was observed for some samples and found to be correlated to the presence of chromium-coated substrates on the substrate holder during the deposition process. In this paper, chromium-free samples have been carefully selected, unless specifically mentioned. Second, the depth profiles of the light elements give evidence of a good superposition of the hydrogen and boron profiles with a tendency to a lower hydrogen surface concentration. The carbon, nitrogen and oxygen impurities appear to be homogeneously distributed over the whole thickness; only in the case of the ^{12}C profile, has a clear additional surface peak (due to the contamination during the ERD measurements) been detected. The apparent shift of the silicon profile into the film is due to the energy straggling of silicon recoils in the boron layer. This straggling results in the degradation of the depth resolution.

The quantitative analysis using the SPME thickness of 106 nm (± 5 nm) yields the following results. The

boron atomic density of 4.94×10^{22} B atoms cm^{-3} is a factor 2.5 lower than the usual crystal density (13×10^{22} B atoms cm^{-3}). The hydrogen atomic density of 0.93×10^{22} H atoms cm^{-3} can also be expressed by the parameter H/B = 0.19; this will be discussed later in relation to the other measurements by hydrogen effusion and infrared spectroscopy. Some uncertainties may arise from the thickness determination. First, the SPME thickness has been checked by the stylus profiling technique which gives $d = 110$ nm. Thus, the most important source of error may arise from the sample thinning due to ion bombardment during the measurement, which may amount to 40 nm; however, the measured surface density of 13.5 μg cm^{-2} is in good agreement with the independent measurement by the Castaing microprobe technique where the samples are less subject to some etching during the measurement.

The integrated profiles result in a mean bulk chemical composition of the atmospherically exposed sample corresponding to $B_{0.64}H_{0.12}O_{0.12}C_{0.06}N_{0.06}$. The chemical composition is found to be constant within the experimental error (0.5%) at the scale of 5–12 months after the deposition. The surface density of 13.5 μg cm^{-2} corresponds to a volume density of 1.36 g cm^{-3} well below the single crystal density of 2.34 g cm^{-3}. These results show an important excess volume of the investigated material in coherence with their high reactivity towards the ambient atmosphere. However, the scale of such an excess volume remains undetermined.

The boron–carbon alloy measured after 1 month exposure to the atmosphere corresponds to the alloy composition $B_{0.34}C_{0.31}O_{0.01}H_{0.34}$ (Fig. 6). Using the SPME thickness $d = 415$ nm ($\pm$ 10 nm), the surface density of 81 μg cm^{-2} yields a volume density of 1.95 g cm^{-3} as compared to the 2.52 g cm^{-3} density of the single crystal B_4C. The higher thickness (as compared to Fig. 5) allows a more precise measurement of the composition profile. In particular, a lower hydrogen content is found again in the near-surface region. The chromium impurity profile is clearly decreasing as the distance from the substrate increases, which may result from some recycling of chromium by the plasma. Two peaks of oxygen impurities are evinced near both interfaces while the bulk oxygen contamination is found to be constant over the whole film thickness; it may be attributed to the low deposition rate and strong affinity of boron towards the oxygen atoms which outgas from the reactor during the deposition process.

3.3.2. Castaing microprobe

The sample studied with ERD (Fig. 5) was also investigated in detail with the Castaing microprobe technique. First, the boron K line profile is found to be very different from that of the single-crystal boron that was recorded under the same experimental conditions. This suggests an important sensitivity to the chemical environment. Second, the surface densities of boron and oxygen atoms are deduced from a simple model which assumes a homogeneous boron–oxygen alloy on a silicon substrate and takes into account the electron stopping efficiencies of the components. In the Castaing microprobe data analysis, the influence of the other impurities has been neglected. Such a model yields results which are in rather good agreement with the experiment when the boron and oxygen surface densities are set to 7.1 and 2.7 μg cm^{-2}, respectively. The oxygen-to-boron atomic ratio O/B = 0.12 is found to be lower than the value deduced from the ERD measurements (0.19). The sample thickness of 62 nm is underestimated because the single-crystal boron density is used. However, the resulting volume density of 1.58 g cm^{-3} is consistent with the ERD value (1.36 g cm^{-3}).

3.3.3. Thermal effusion

Fig. 7 shows the typical effusion curves obtained from boron films deposited at 50 and 100 °C and exposed to the atmosphere for 3 months. The effusion curves are composed of two peaks, the lower temperature peak, being much weaker, appears as a shoulder at 270 °C, while the high-temperature peak is centred around 350–400 °C. The threshold effusion temperature, $T_t = 150$ °C, and the temperature of the first effusion peak are not very sensitive to the deposition temperature in the range 50–100 °C. The shift towards lower effusion temperatures from 390 to 360 °C as a function of the deposition temperature, T_s, may also result from uncontrolled chromium incorporation in the sample deposited at 100 °C, as shown by ERD measurements on the same samples. A tail of hydrogen effusion up to 700 °C is observed for samples in the 0.1–1.1 μm thick range, which indicates the presence of a small fraction of stable sites for hydrogen atoms in the reconstructed network. From the integrated curves of Fig. 7 and the sample thickness, the hydrogen atomic densities of 1.3

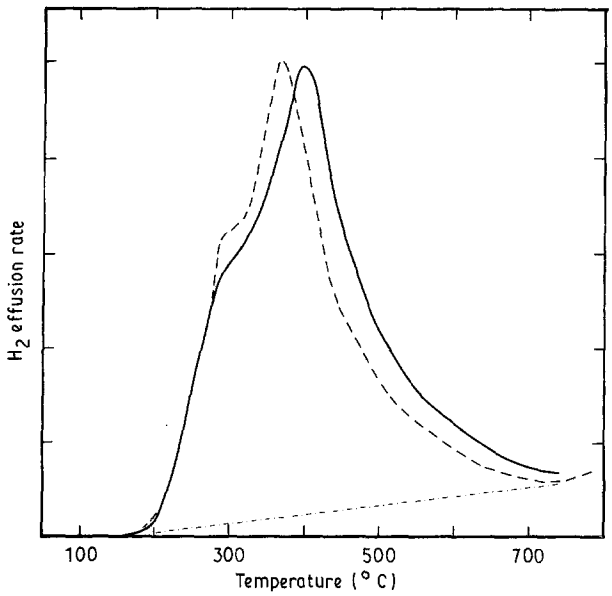

Figure 7 Typical thermal effusion of hydrogen from hydrogenated amorphous boron films deposited at $T_s = 50$ °C, $d = 0.62$ μm (——) and $T_s = 100$ °C, $d = 1.0$ μm (– – –). The spectra are normalized to the maximum effusion rate.

$\times 10^{22}$ and 0.95×10^{22} H atoms cm^{-3} were deduced for $T_s = 50$ and 100 °C, respectively. Much lower concentrations (by a factor of 2) have been found in the samples with a chromium contamination.

3.3.4. Structural characterization

In order for us to obtain more insight into the material structure, thin films in the range 150–270 nm were deposited simultaneously on carbon-coated nickel grids and on cleavage surfaces of NaCl single crystals. The latter were afterwards floated on distilled water and picked up on molybdenum grids. A thin gold film was evaporated on half of one sample as an internal standard for diffraction measurements. Transmission electron microscope (TEM) observations, as well as selected-area diffraction patterns (SAD) performed on a Phillips CM 30 microscope, showed that the films were uniform and amorphous. Measurements of some of the diffraction patterns made in an optical microdensitometer (Fig. 8) gave the following values for the observed maxima: 0.438, 0.247 and 0.140 nm, in reasonable agreement with reported values for amorphous boron [29, 34]. Some samples were annealed *in situ*; although the films always cracked between 400 and 500 °C, enough areas remained suitable for observation which shows that they were amorphous up to approximately 950 °C. However, in many of the specimens the inner diffraction halo could not be resolved from the directly transmitted beam; the outer two did not differ appreciably from those reported for B_2O_3 [35].

It can be noticed that the cracking occurs near the melting temperature for boric oxide glass B_2O_3 [36]. In addition, after the thermal effusion treatment, and a 4 month exposure to the atmosphere, the films show a strong infrared absorption band at 1390 cm^{-1} consistent with the B_2O_3 material [26] and a low contribution of B–O–H vibrations, which indicates a lower reactivity with the ambient moisture after annealing. Both results show that the high-temperature behaviour also depends strongly on the oxygen affinity of boron atoms, the B–O bond energy being as high as 193.3 kcal mol^{-1}.

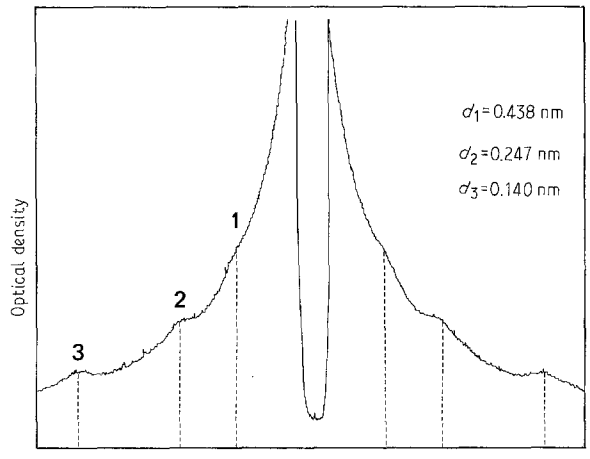

Figure 8 Optical microdensitometer recording of the electron diffraction pattern of a specimen deposited on a carbon film: optical density as a function of the distance from the center of the diffraction pattern ($\sin\theta/\lambda$ arb. units).

4. Conclusion

The amorphous boron–hydrogen alloys deposited at low deposition rate (0.014 nm s^{-1}) and low temperatures (50–100 °C) by the glow-discharge decomposition of diborane B_2H_6 diluted in hydrogen have been studied with respect to their optical properties and chemical composition as well as their reactivity with the ambient atmosphere.

The electron microscope pictures show homogeneous samples with no large-scale microstructures and the electron diffraction analysis of the haloes is consistent with the positions found for the amorphous boron. The optical properties of the amorphous hydrogenated boron films are characteristic of the high optical gap semiconductors, the 1 μm thick films being transparent in the visible spectrum. Typical values for the optical gap E_{04} (energy corresponding to an absorption coefficient of 10^4 cm^{-1}) and static refractive index are, respectively, found in the range 3.4–4.2 eV and 1.63–1.67. These boron–hydrogen alloys are characterized by a high hydrogen content in the range $0.9–1.3 \times 10^{22}$ H atoms cm^{-3} and a low boron atomic density as given by the elastic recoil detection analysis, namely about 5×10^{22} B atoms cm^{-3} as compared to the usual crystalline boron density (13×10^{22} B atoms cm^{-3}). The lower surface hydrogen content may explain some inaccuracies when using the SPME homogeneous thin film model to describe the optical properties.

Some oxygen atoms, likely due to the reactor outgassing, are quantitatively incorporated during the slow deposition process, while some incorporation of metallic impurities has been correlated to the presence of chromium-coated substrates on the substrate holder. In addition, the as-deposited films react with the ambient atmosphere, so that the films reach a final composition close to $B_{0.64}H_{0.12}O_{0.12}C_{0.06}N_{0.06}$; the ERD profiles show that the impurities are distributed over the whole film thickness. Such a high reactivity with the ambient moisture can be explained by a high excess volume of the layers and a strong oxygen affinity of the boron atoms. A similar modification of the boron films, resulting in a weight increase of the samples at the scale of a few hours, has been observed previously [2, 12]. The infrared spectroscopy measurements give evidence of the B–H terminal- and B–H–B bridge-bonds' absorption in the as-deposited films; as the hydrolysis of the boron–hydrogen alloy takes place, the progressive vanishing of the bridge bonds and the increase of the B–H and B–O–H bonds occur. Some particular deposition conditions, such as the CVD deposition technique above 290 °C, yield an as-deposited material with no B–H–B or B–O–B bridge bonds and with no detectable oxidation or hydrolysis in the ambient atmosphere [5]. Thus, the occurrence of bridge bonds in the as-deposited material might be related to the poor stability of the hydrogenated boron thin films.

In comparison, the amorphous hydrogenated boron–carbon alloy of composition $B_{0.34}C_{0.31}O_{0.01}H_{0.34}$ deposited at 250 °C is found to have a lower optical gap and a higher refractive index; the higher atomic density found by ERD is consistent with a lower oxygen incorporation after the deposition.

Acknowledgements

We thank J. L. Pouchou for the Castaing microprobe measurements performed at the ONERA laboratories, Châtillon, France, and for stimulating discussions, Satyendra Kumar for the ellipsometry measurements and J. Perrin for valuable discussions. We are also grateful to D. Conne, J. Huc and M. J. Surmont for the technical assistance and the preparation of the graphs.

References

1. H. TOYODA, H. SUGAI, T. ISOZUMI and T. OKUDA, *Appl. Phys. Lett.* **51** (1987) 798.
2. S. VEPREK, S. RAMBERT, M. HEINTZE, M. MATTENBERGER, M. JURCIK-RAMAN, W. PORTMANN, D. RINGER and U. STIFFEL, *J. Nucl. Mater.* **162–164** (1989) 724.
3. A. RAVEH, A. INSPEKTOR, U. CARMI and R. AVNI, *Thin Solid Films* **108** (1983) 39.
4. L. J. DIMMEY, H. PARK, P. L. JONES and F. H. COCKS, *J. Electron. Mater.* **10** (1981) 111.
5. B. G. BAGLEY, D. E. ASPNES, A. C. ADAMS and R. E. BENENSON, *J. Non-Cryst. Solids* **35, 36** (1980) 441.
6. C. C. TSAI, *Phys. Rev. B* **19** (1979) 2041.
7. H. O. PIERSON and A. MULLENDORE, *Thin Solid Films* **83** (1981) 87.
8. N. A. BLUM, C. FELDMAN and F. G. SATKIEWICZ, *Phys. Status Solidi (a)* **41** (1977) 481.
9. K. KATADA, *Jpn J. Appl. Phys.* **5** (1966) 582.
10. R. WEIL, I. ABDULHALIM, R. BESERMAN, M. JANAI and B. PRATT, *J. Non-Cryst. Solids* **77, 78** (1985) 261.
11. I. FREUND and R. S. HALFORD, *J. Chem. Phys.* **43** (1965) 3795.
12. C. BRAGANZA, S. VEPREK and P. GRONER, *J. Nucl. Mater.* **85–86** (1979) 1133.
13. P. ROCA i CABARROCAS, B. EQUER, J. HUC, A. LLORET and J. P. M. SCHMITT, in "7th EC Photovoltaic Solar Energy Conference", Seville, 1986, edited by A. Goetzberger, W. Palz and G. Willeke (Reidel, Dordrecht, 1986) p. 533.
14. B. DREVILLON, J. PERRIN, R. MARBOT, A. VIOLET and J. L. DALBY, *Rev. Sci. Instrum.* **53** (1982) 969.
15. G. SARDIN, J. ANDREU, J. C. DELGADO, J. ESTEVE and J. L. MORENZA, in "7th EC Photovoltaic Solar Energy Conference", Seville, 1986, edited by A. Goetzberger, W. Palz and G. Willeke (Reidel, Dordrecht, 1986) p. 577.
16. J. L. POUCHOU, in "Proceedings of the 1st European Workshop on Modern Developments and Applications in Microbeam Analysis", Anvers, 1989, edited by EMAS and UIA. J. L. Pouchou and F. Pichoir, *Scanning* **12** (1990) 212.
17. J. L'ECUYER, C. BRASSARD, C. CARDINAL and B. TERREULT, *Nucl. Inst. Methods* **49** (1978) 271.
18. S. C. GUJRATHI, P. AUBRY, L. LEMAY and J. P. MARTIN, *Canad. J. Phys.* **65** (1987) 950.
19. R. GROLEAU, S. C. GUJRATHI and J. P. MARTIN, *Nucl. Inst. Methods Phys. Res.* **B218** (1983) 11.
20. K. OXORN, S. C. GUJRATHI, S. BULTENA, L. CLICHE and J. MISKIN, *ibid.*, **B45** (1990) 166.
21. G. K. RIBBEGARD and R. N. JONES, *Appl. Spectrosc.* **34** (1980) 638.
22. A. ANTOINE, B. DREVILLON and P. ROCA i CABARROCAS, *J. Appl. Phys.* **61** (1987) 2501.
23. D. E. ASPNES and A. A. STUDNA, *Phys. Rev. B* **27** (1983) 985.
24. A. A. BEREZIN, O. A. GOLIKOVA, M. M. KAZANIN, T. KHOMIDOV, D. N. MIRLIN, A. V. PETROV, A. S. KUMAROV and V. K. ZAITSEV, *J. Non-Cryst. Solids* **16** (1974) 237.
25. F. H. COCKS, P. L. JONES and L. J. DIMMEY, *Appl. Phys. Lett.* **36** (1980) 970.
26. J. L. PARSONS and M. E. MILBERG, *J. Amer. Ceram. Soc.* **43** (1960) 326.
27. W. ZIMMERMAN III, A. M. MURPHY and C. FELDMAN, *Appl. Phys. Lett.* **10** (1967) 71.
28. T. C. DEVORE, J. R. WOODWARD and J. L. GOLE, *J. Phys. Chem.* **92** (1988) 6919.
29. R. G. DELAPLANE, U. DALHBORG, W. H. HOWELLS and T. LUNDSTROM, *J. Non-Cryst. Solids* **106** (1988) 66.
30. W. WEBER and M. F. THORPE, *J. Phys. Chem. Solids* **36** (1975) 967.
31. M. H. BRODSKY, M. CARDONA and J. J. CUOMO, *Phys. Rev. B* **16** (1977) 3556.
32. H. SHANKS, C. J. FANG, L. LEY, M. CARDONA, F. J. DEMOND and S. KALBITZER, *Phys. Status Solidi (b)* **100** (1980) 43.
33. S. C. SHEN and M. CARDONA, *Phys. Rev. B* **23** (1981) 5322.
34. M. KOYABASHI, *J. Mater. Sci.* **23** (1988) 4392.
35. J. ZARZICKI, "Les verres et l'état vitreux" (Masson, Paris, 1982) p. 79.
36. "CRC Handbook of Chemistry and Physics", 69th Edn, edited by R. C. Weast (CRC Press, Boca Raton, Florida) pp. B 77 and F 174.

Received 24 July 1990
and accepted 6 February 1991